

Polythiophene-wrapped Chitosan Nanofibrils with a Bouligand Structure toward Electrochemical Macroscopic Membranes

Nhan Thi Thanh Dang,* Thang Quoc Le, Nguyen Duc Cuong, Nguyen Le My Linh, Lam Son Le, Tien Dong Tran, and Hai Phong Nguyen



Cite This: *ACS Omega* 2024, 9, 13680–13691

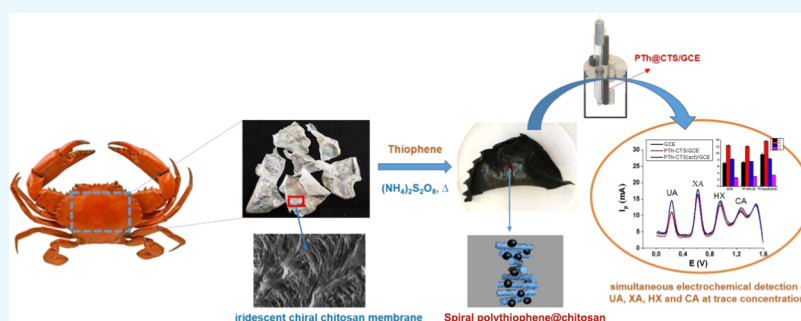


Read Online

ACCESS |

Metrics & More

Article Recommendations



ABSTRACT: Exploring structural biomimicry is a great opportunity to replicate hierarchical frameworks inspired by nature in advanced functional materials for boosting new applications. In this work, we present the biomimetic integration of polythiophene into chitosan nanofibrils in a twisted Bouligand structure to afford free-standing macroscopic composite membranes with electrochemical functionality. By considering the integrity of the Bouligand structure in crab shells, we can produce large, free-standing chitosan nanofibril membranes with iridescent colors and flexible toughness. These unique structured features lead the chitosan membranes to host functional additives to mimic hierarchically layered composites. We used the iridescent chitosan nanofibrils as a photonic platform to investigate the host–guest combination between thiophene and chitosan through oxidative polymerization to fabricate homogeneous polythiophene-wrapped chitosan composites. This biomimetic incorporation fully retains the twisted Bouligand organization of nanofibrils in the polymerized assemblies, thus giving rise to free-standing macroscopic electrochemical membranes. Our further experiments are the modification of the biomimetic polythiophene-wrapped chitosan composites on a glassy carbon electrode to design a three-electrode system for simultaneous electrochemical detection of uric acid, xanthine, hypoxanthine, and caffeine at trace concentrations.

INTRODUCTION

Electrically conductive polymeric materials are renowned as a key component in the electronics industry to develop optical and electronic devices.^{1,2} Considering their advantage over robust metal conductors, the mechanical flexibility and electron-transition capacity are unique features of such promising materials to fabricate bendable and stretchable organic electronics.^{3,4} Manipulating the polymer assembly, hierarchical structures, and desirable composition at the microscopic and nanoscale levels are essential to achieve advanced functional materials with greater performance and processability for technological applications.^{5,6} With the exception of the intrinsic electrical conductivity, the conducting polymer materials have a wide range of applications in the electrochemical field.^{7,8} Recent studies on combining polymer chemistry with structural biomimicry have created incredible organic electronics that can act as probes, electronic skins, solar cells, and switchable sensors.^{9,10} Because of this interest, tremendous efforts in

innovating materials and approaches are vital to boost the functionality and efficiency of electrically conductive polymer-based composites.¹¹

Polythiophene is a π -conjugated polymer is of great interest in photoelectric device applications due to electrical conductivity of up to 100 S/cm, thermal/chemical stability, and synthetic feasibility.^{12,13} The presence of conjugated double bonds along the backbone creates the electrical conductivity in the π -conjugated polymer (e.g., polythiophene).¹⁴ The π electrons in the conjugated backbone are delocalized into a conduction band, thus giving rise to the metallic behavior.¹³ Chemical and/

Received: October 9, 2023
Revised: February 22, 2024
Accepted: February 27, 2024
Published: March 15, 2024



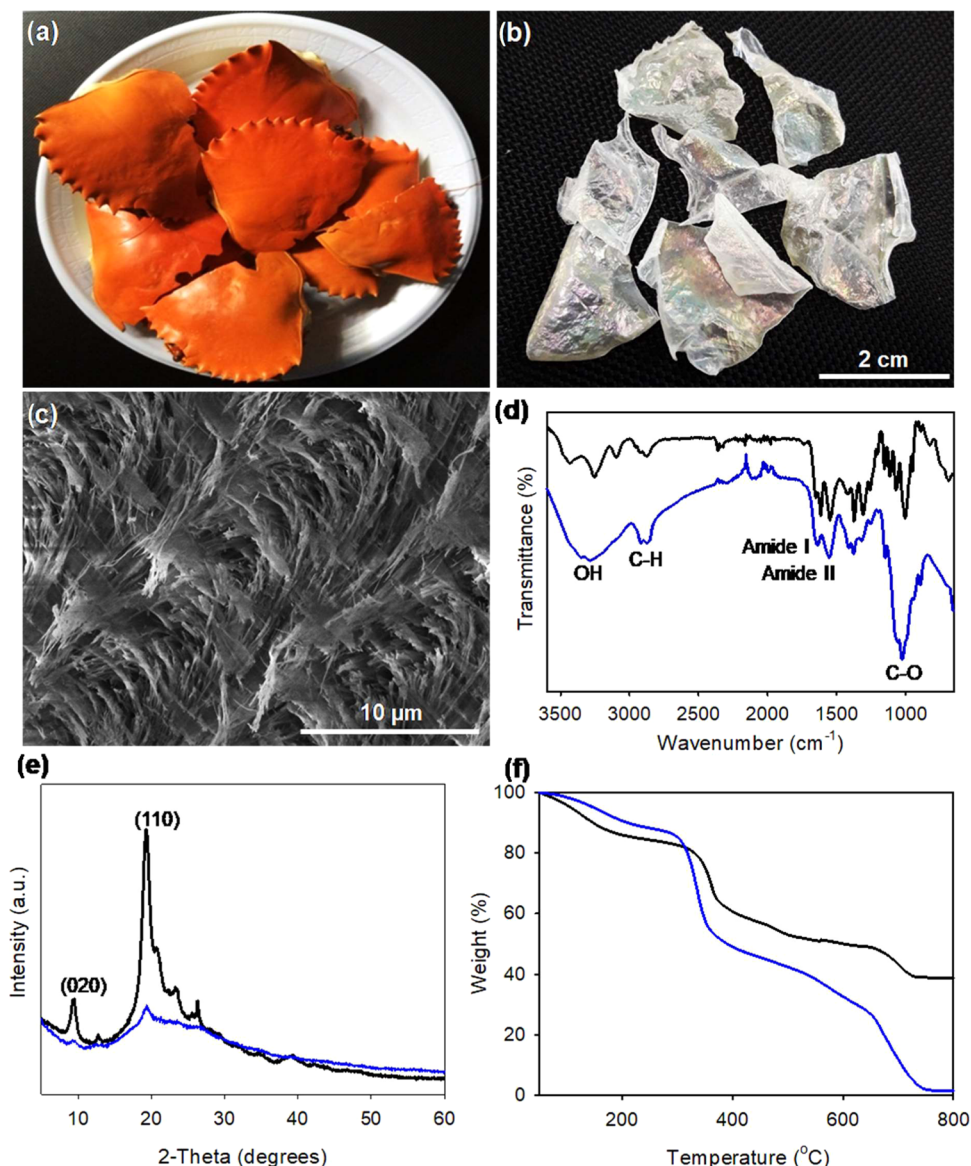


Figure 1. Free-standing macroscopic chitosan nanofibril membranes with structural colors and mechanical flexibility. (a) Photo of cooked crab shells, (b) photo of iridescent chitosan membranes derived from crab shells, (c) SEM image of chitosan membrane, (d) IR spectra of chitin (black line) and chitosan (blue line), (e) PXRD patterns of chitin (black line) and chitosan (blue line), and (f) TGA curves of natural crab shell (black line) and chitosan (blue line) at $10\text{ }^{\circ}\text{C min}^{-1}$ under an air atmosphere.

or electrochemical methods can be used to synthesize polythiophene with the controllability of structural forms such as thin films, porous networks, fibers, and particle colloids.^{15–17} Among π -conjugated polymers such as polypyrrole, polyaniline, and poly(3,4-ethylenedioxythiophene) (PEDOT), polythiophene-based materials have been widely investigated computationally and experimentally to explore their electrochemical properties for applications in analytical electrodes, light-emitting diodes, biosensors, actuators, and energy storage and conversion.^{18–21} Recently, much progress has been made in using electrical conductive polymeric materials for biomedical applications in biosensors, tissue engineering, soft actuator, and biomedical implants.^{16,22–23,24} However, the poor mechanical reinforcement and low biocompatibility of polythiophene are obstacles to integration into bifunctional systems. To address this limitation, the homogeneous incorporation of biopolymers into polythiophene is an alternative pathway to

obtain multifunctional composites with electrochemical response and biological compatibility.^{25–28}

Chitosan is a derivative of chitin obtained by deacetylation of chitin found in the shells of crustaceans and insects, cell walls in fungi, and among other sources.²⁹ Native chitin nanofibers are highly crystalline but undergo deacetylation by hot alkali treatment to yield soft chitosan networks with low crystallinity.^{30,31} The accessibility of reactive surface-exposed amine groups of chitosan makes them easy to functionalize with additives.³² This is an interesting way to introduce attractive properties, such as electrical conductivity, into biodegradable polymers.³³ Chitosan nanofibrils are promising scaffold materials for biomedical applications.^{34,35} The high porosity, large surface area, large interface, and soft network lead chitosan biopolymer to host π -conjugated polymers beneficial for enhanced performance of the electrical conductivity and mechanical strength.^{36–38} Over the past few decades, extensive studies on the combination of π -conjugated polymers with

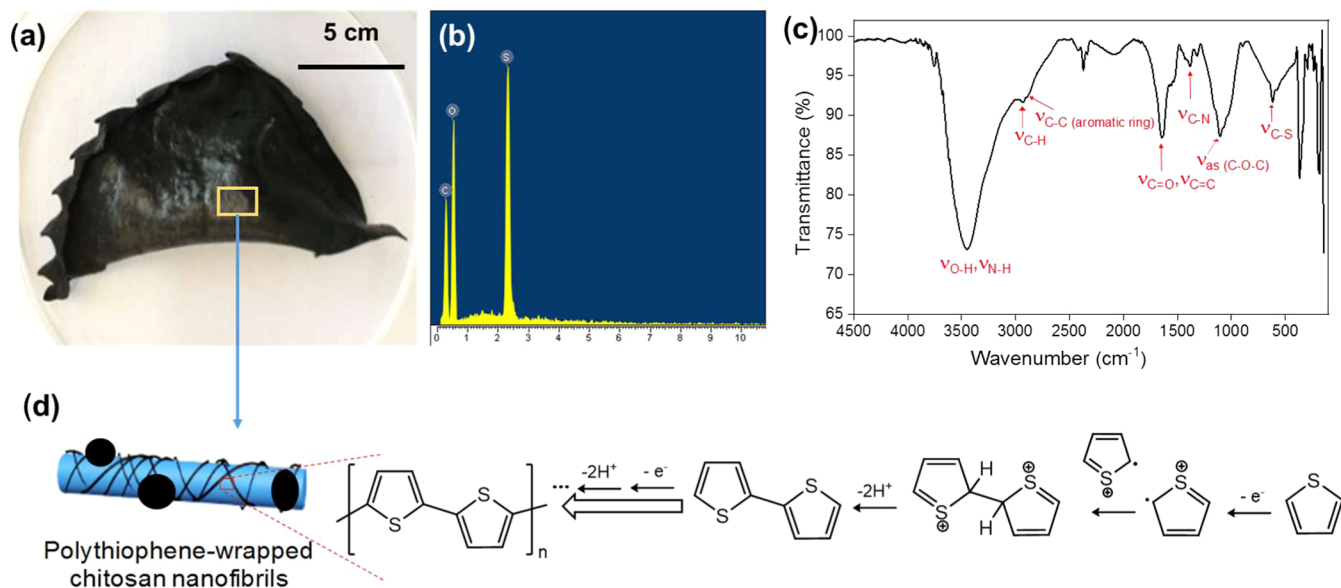


Figure 2. (a) Photo of the free-standing polythiophene/chitosan composite membrane, (b) EDX pattern and (c) IR spectrum of the polythiophene/chitosan composite, and (d) reaction scheme of the oxidation polymerization of thiophene onto chitosan nanofibrils in the porous membrane.

chitosan into conducting composites have been reported.^{39–41} However, the inspiration of polythiophene/chitosan assemblies in a photonic Bouligand membrane on the macroscopic scale for electrochemical sensors is underdeveloped.

Herein, we presented the structural integration of polythiophene and chitosan into a free-standing macroscopic membrane with a Bouligand structure. The homogeneous polythiophene/chitosan composite membrane shows great mechanical toughness arising from the naturally cross-linked hierarchical networks of chitosan nanofibrils. Uric acid (UA), xanthine (XA), and hypoxanthine (HX) are degradation products of purine metabolism in human beings, and caffeine (CA) is generally introduced to the body through food, soft drinks, and/or medicines. Developing analytical methods to simultaneously determine these intermediate compounds is thus essential for investigating the homeostasis of the oxidase system and clinical diagnosis at the early stages of the related diseases.^{42,43} Beyond the synthetic effort, we evaluated the electrochemical properties of the resulting polythiophene/chitosan composites by designing them as electrodes for simultaneous analysis of these four organic compounds at trace concentrations.

RESULTS AND DISCUSSION

We prepared iridescent chiral nematic mesoporous chitosan from discarded crab shells obtained from local seafood sources (Figure 1a). In a typical preparation, the natural crab shells were deproteinized using a hot dilute base and then demineralized by fresh dilute acid to extract the pure chitin nanofibrillar shell-like membrane. The resulting chitin was treated with hot concentrated alkali at 90 °C to release acetyl groups, called deacetylation, and a flexible chitosan membrane was obtained. To transform the layered hierarchy into layered chirality, the resulting chitosan was treated repeatedly with hot 50 wt % NaOH aqueous solution at least three times to relax its hierarchical nanofibril assemblies, and consequently, the iridescent chiral nematic chitosan membrane can be formed (Figure 1b). The chemical purification of the crab shell fully released the protein and mineral components embedded within

the nanofibril assemblies to open nanosized spaces in the hierarchical networks, thus forming porous chitosan membranes. The chitosan membrane is semitransparent, flexible, and exhibit water swelling compared to pristine chitin, resulting from the formation of its hydrophilic soft network. Thermogravimetric analyses (TGA) showed that the chitosan membrane is stable up to around 350 °C in an air atmosphere and completely decomposes beyond 700 °C, whereas the crab shell sample leaves around 40 wt % calcium-based minerals (Figure 1f).

Infrared spectra (Figure 1d) of the chitosan show bands at 3550–3200 cm^{-1} for O–H and N–H stretching, at 2920–2886 cm^{-1} for C–H stretching and 1078–1072 cm^{-1} for C–O–C/glycoside stretching. Moreover, the IR spectra also show peaks at $\sim 1665 \text{ cm}^{-1}$ for C=O (amide I) stretching and at $\sim 1570 \text{ cm}^{-1}$ for N–H bending, and 1317 cm^{-1} for C–N (amide II) bending, where the amide I/amide II ratio in the chitosan is lower than that in chitin. This suggests the deacetylation of chitin occurred to generate chitosan.³⁰ Powder X-ray diffraction (PXRD) analyses (Figure 1e) showed that chitosan has typical peaks at 9.2 and 19.5° 2θ corresponding to (020) and (110) planes that are the same positions as those in pristine chitin, but their diffraction intensity is weaker.³⁰ This indicates that the deacetylation originally preserved the structural phase of chitosan but its crystallinity considerably decreased. Scanning electron microscopy (SEM) images (Figure 1c) of the chitosan membrane show nanofibrils with diameters of 5–20 nm and lengths of up to several hundred micrometers in hierarchical assembled networks. The chitosan nanofibrils spiral along the helical axis in a clockwise direction through the thickness to create a left-handed chiral nematic structure in the mesoporous membrane. This structural organization is also known as the Bouligand structure, which resembles the layered twisting of chitin nanofibrils in jewel beetle shells.⁴⁴ The periodic helicity of the chitosan nanofibrils establishes a specific pitch in the visible region ($\sim 500\text{--}700 \text{ nm}$) to show iridescent colors as a result of the diffraction of incident light with the membrane. The comparative analyses of the PXRD and SEM results suggest that the hot alkali-induced deacetylation diminishes the hydrogen bonding of chitosan intra- and intermacromolecules to relax its

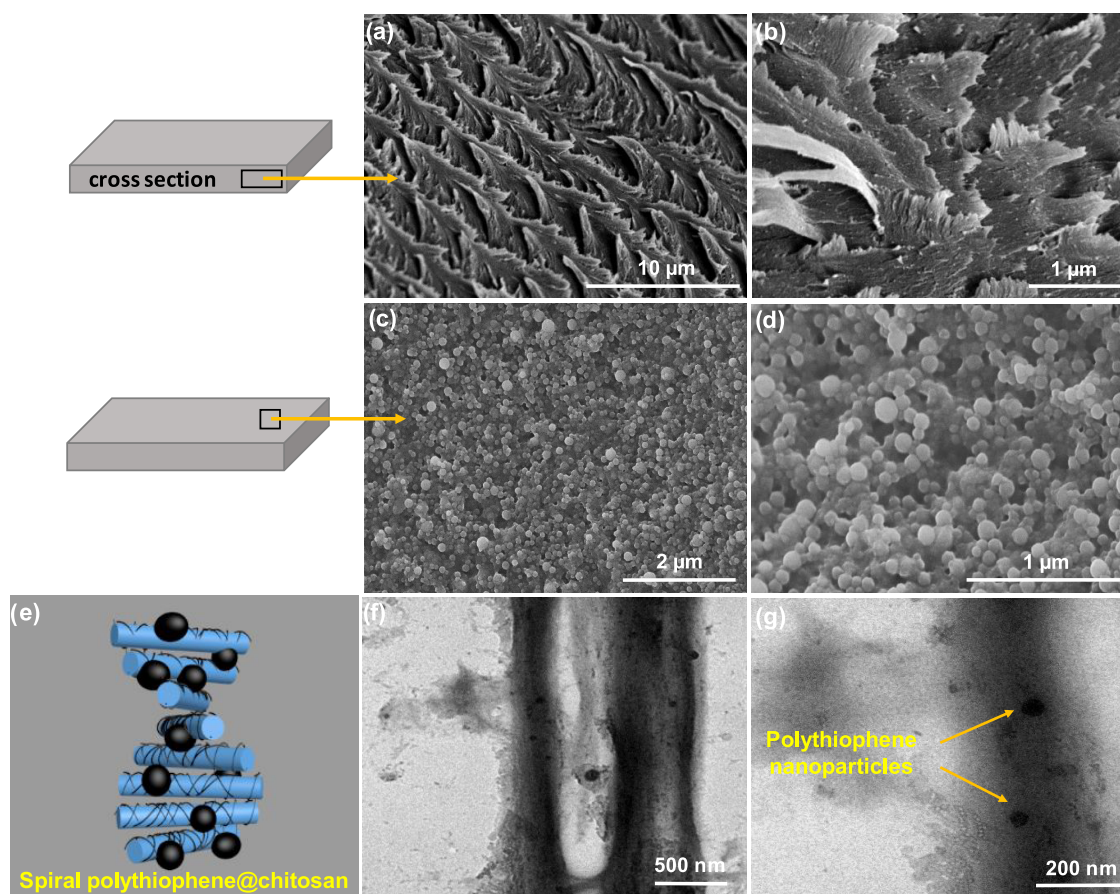


Figure 3. Structural organization of polythiophene/chitosan nanofibrils in a macroscopic membrane. SEM images of fractural cross-section of the composite membrane at low (a) and high (b) magnifications and SEM images of the top surface of the composite membrane at low (c) and high (d) magnifications. (e) Structural model of the nanoscale twist of polythiophene/chitosan nanofibrils, and (f, g) TEM images of polythiophene/chitosan nanofibrils at two different magnifications.

naturally assembled network, thus deforming the layered twisting from the layered hierarchy.

Thanks to the nanoscale, porosity, hierarchy, flexibility, and sustainability, the free-standing photonic chitosan membranes are an exceptional form of biopolymers to access its potential use as a helicoidal platform for inspiring advanced functional materials.^{45–47} Such inspirational research is possible because the functional amine groups available on the chitosan nanofibrils can molecularly complex with additives, such as polymers, nanoparticles, and organic compounds. Electrically conducting polymers are attracting particular interest from academic and industrial researchers to develop electrochemical technologies in sensors and energy storage devices.^{48,49} Considering this unprecedented combination, we investigated the host–guest combination between polythiophene and chitosan to construct electrochemically bioinspired probes that are macroscopic composite membranes with free-standing and sustainable features.

We used iridescent chitosan membranes to host polythiophene through a polymeric combination. Typically, the mesoporous chitosan membranes were treated with thiophene in the presence of ammonium persulfate as an oxidizing agent at 60 °C to proceed with the oxidation polymerization and polymer incorporation. Under these identical reaction conditions, the thiophene monomers were polymerized and coated around the nanofibrils to generate 314 mg of black, free-standing polythiophene-wrapped chitosan composite membranes in

which the ratio of polythiophene and chitosan is 1:3 (%w/w). The black polythiophene/chitosan composite fully retains the iridescence characteristic of the chiral nematic structure (Figure 2a). The composite is more mechanically reinforced than the pristine sample arising from the formation of the heterogeneous polythiophene/chitosan networks. The PTh/CTS membrane slightly swells when soaked or sonicated in water, and no PTh particles detached from the PTh/CTS membrane into the water. This indicates that there has been a strong interaction between CTS and polythiophene that is difficult to release. The cross-section EDX analysis results of PTh/CTS membrane (Figure 2b) show the presence of C, O, and S inside the as-prepared material. These are the constituent elements of CTS and polythiophene. IR spectral analyses (Figure 2c) of the composites revealed the remaining characteristic stretches of the amide and carbonyl groups for chitosan and the remarkable appearance of a new typical peak at ~ 2932 , 1645, and 617 cm^{-1} assigned to the C–C stretching between two aromatic rings, C=C stretching, and C–S stretching vibration of thiophene rings, respectively.^{30,50,51} Especially, the peak observed at 1317 cm^{-1} is the signal of the C–N stretching vibration of the aromatic compound. This verifies the incorporation of polythiophene onto the chitosan matrix in the structured composites (Figure 2d).

The organized structure of the polythiophene/chitosan composite was assessed by SEM as shown in Figure 3a–d. The overall morphology of the chiral nematic chitosan structure

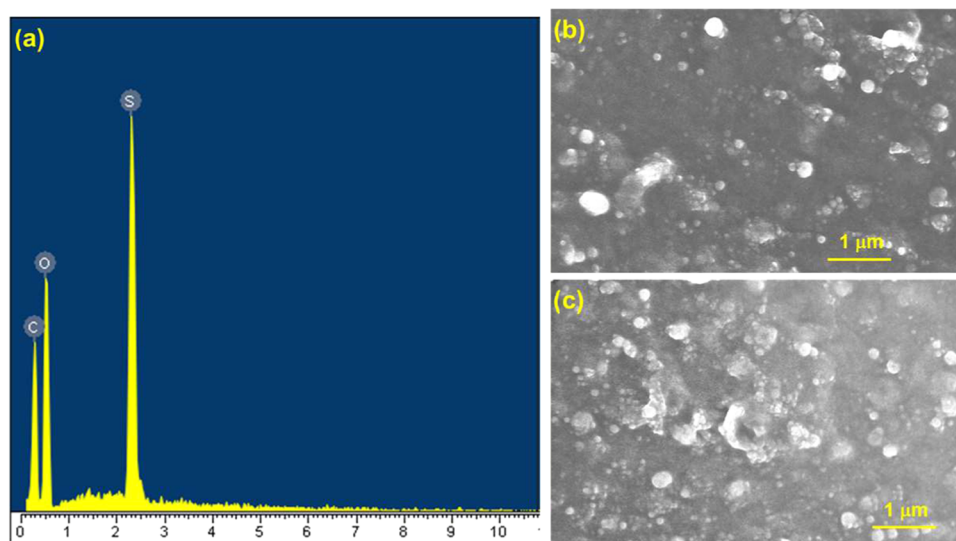


Figure 4. (a) EDX pattern and SEM images of PTh-CTS on the surface of GCE before (b) and after (c) electrochemical analysis.

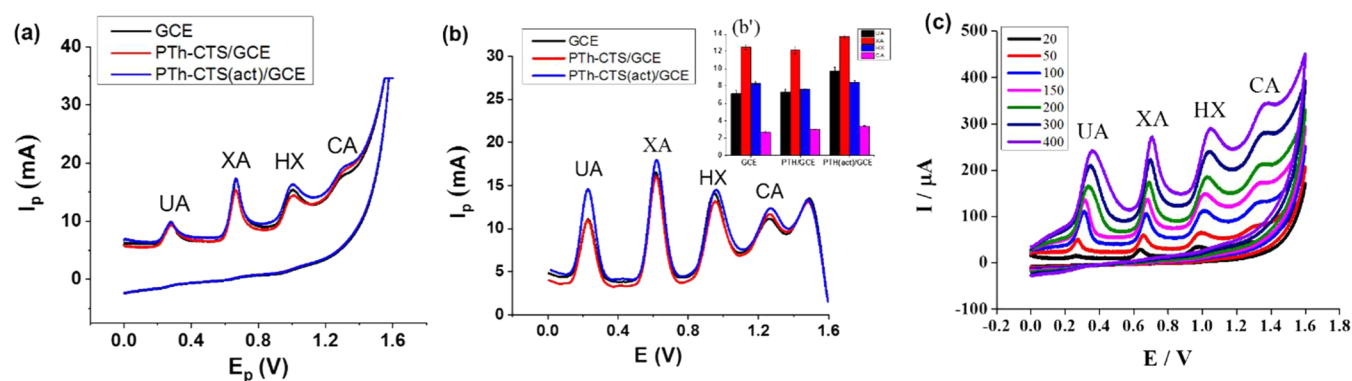


Figure 5. (a) CV and (b) DP-ASV voltammograms for 3×10^{-4} M solution of UA, XA, HX, and CA in 0.04 M BRB (pH = 7.0) on GCE, polythiophene-wrapped chitosan/GCE, and activated polythiophene-wrapped chitosan/GCE; inset of (b) is the peak intensity of GCE, polythiophene-wrapped chitosan/GCE, and activated polythiophene-wrapped chitosan/GCE in the DP-ASV method. The accumulation experimental conditions are $t_{\text{acc}} = 10$ s, $E_{\text{acc}} = -0.9$ V, $\nu = 20$ mV s $^{-1}$, and DP-ASV condition is $\Delta E = 60$ mV. (c) Cyclic voltammogram profile of 4×10^{-4} M solutions of UA, XA, HX, and CA in 0.04 M BRB (pH = 7) on the activated polythiophene-wrapped chitosan/GCE at different scan rates. CV conditions are $t_{\text{acc}} = 10$ s and $E_{\text{acc}} = -0.9$ V.

was originally preserved upon thiophene polymerization, of which we saw the features of nanofibrils, layers, and helicity characteristic of the Bouligand-type organization.^{30,52} The formation of polythiophene onto the chitosan networks can be observed by SEM. In fractural cross sections, the incorporation of polythiophene polymers into the confined chitosan assemblies is homogeneous, and thus, its tiny particles formed could not be distinguished. As a result, a homogeneous polythiophene-grafted chitosan network with nanoscale helicity presents through membrane's thickness (Figure 3a,b). More evidently, we can observe numerous 50–150 nm-sized polythiophene nanoparticles deposited onto the surfaces of the chitosan membrane (Figure 3c,d). This size-selective deposition is reasonable for seed-mediated growth, where small polythiophene nanoparticles grew limitedly inside the assembled membrane by its compacted nanofibril structure, while the overgrowth occurred on the membrane surfaces to form larger polythiophene nanoparticles. Transmission electron microscopy images (Figure 3f,g) further confirm that the polymerized membrane is a composite made of polythiophene nanoparticles deposited onto chitosan nanofibrils.

We investigated the electrochemical properties of the polythiophene/chitosan composites by designing them as an analytic electrode to simultaneously determine the trace amount of UA, XA, HX, and CA using a different pulse anodic stripping voltammetry (DP-ASV) technique. A three-working electrode system was set up with the function of GCE, polythiophene-wrapped chitosan/GCE (PTh-CTS/GCE), and activated polythiophene-wrapped chitosan/GCE (PTh-CTS(act)/GCE) as working electrodes. PTh-CTS/GCE was prepared by coating the dispersion of the polythiophene/chitosan composite on the cleaned GCE surface followed by drying. The morphology of the surface of PTh-CTS/GCE before and after electrochemicals were evaluated by EDX and SEM. The EDX pattern of the modified electrode (Figure 4a) indicated the presence of C, O, and S with atomic contents of 51.98, 42.68, and 5.34%, respectively. The SEM images of PTh-CTS (Figure 4b,c) showed little change on the surface of GCE before and after electrochemical analysis.

The cyclic voltammetry (CV) response of bare GCE, PTh-CTS/GCE, and PTh-CTS(act)/GCE was investigated by 10 mL of 40 mM BRB solution at pH 7.0 containing HX, XA, UA, and CA with desired concentrations (Figure 5a,b). The initial

testing showed that all three electrodes are electrochemically active to all four analytes as four anodic signals can be distinguishable for UA, HX, XA, and CA. However, the activated polythiophene-wrapped chitosan/GCE electrode gives the highest current intensity and better repeatability compared to the polythiophene-wrapped chitosan/GCE and bare GCE electrodes, indicating its most active electrochemical performance. The current intensities according to the four peaks due to UA, XA, HX, and CA in the three electrodes including GCE, PTh-CTS/GCE, and PTh-CTS (act)/GCE are given in Table 1.

Table 1. Current Intensities of the Three Electrodes According to the Four Analytes UA, XA, HX, and CA

| | UA | XA | HX | CA |
|-------------------|-----|------|-----|-----|
| GCE | 7.1 | 12.5 | 8.3 | 2.7 |
| PTh-CTS/GCE | 7.3 | 12.1 | 7.6 | 3.0 |
| PTh-CTS (act)/GCE | 9.7 | 13.7 | 8.5 | 3.4 |

This suggests that the electrochemical activation could be mostly related to the reduction of oxygenated groups in the anode material to make the electrode more active and conductive, and consequently, the electron and mass transfer process is promoted to exhibit better electrochemical catalytic behavior. Evidently, the incorporation of polythiophene into the chitosan matrix plus the additional step of the electrochemical activation provides an essential conduction pathway to prepare the active voltammetric electrodes. As a result, we selected the activated polythiophene-wrapped chitosan/GCE electrode to prove the potential application in the electrochemical analysis to simultaneously detect UA, HX, XA, and CA at trace concentration levels.

The effect of the pH range is very important, and it is essential to select the desired pH value. The effect of pH on the voltammetry response of the activated polythiophene/chitosan/GCE electrode was investigated in the pH range of 2.0–9.0 in the 40 mM BRB solution containing 4.10^{-4} M each of UA, XA, HX, and CA. As shown in Figure 6a, in the pH range of 5.0–9.0 the prepared electrode can detect simultaneously these four analytes to show four characteristic signals fully separated from each other. However, the anodic peak current increased as the pH was changed from 2.0 to 9.0, reaching a maximum intensity with well-defined peaks at pH 7.0, and then decreased dramatically down to pH 9.0. As shown in Figure 6b,c, the corresponding calibration curves for UA, XA, HX, and CA were built from pH 2.0 to pH 9.0. The linearization equations were $E_{p,UA} = (0.641 \pm 0.013) + (-0.060 \pm 0.002)pH$, $E_{p,XA} = (1.011 \pm 0.013) + (-0.057 \pm 0.002)pH$, $E_{p,HX} = (1.400 \pm 0.034) + (-0.063 \pm 0.005)pH$, and $E_{p,CA} = (1.306 \pm 0.028) + (-0.008 \pm 0.004)pH$, with the corresponding correlation coefficients of $-0.060 (\pm 0.002)$, $-0.057 (\pm 0.002)$, $-0.063 (\pm 0.005)$, and $-0.008 (\pm 0.004)$ for UA, XA, HX, and CA, respectively. It is suggested that the increase in the peak current when the pH was changed from 2.0 to 9.0 is due to the electrostatic attraction and the complexation mechanism. We believe that the hydroxyl, amine, and thiol groups act as affinity sites to adsorb the small organic compounds (UA, XA, HX, CA) on the polythiophene-wrapped chitosan/GCE electrode surface to increase the pK_a range. The decrease in the stripping signals at a higher pH value of 7.0 may be related to the aggregation of the analytes. Thus, a pH of 7.0 in the 40 mM BRB solution was employed in further electrochemical experiments.

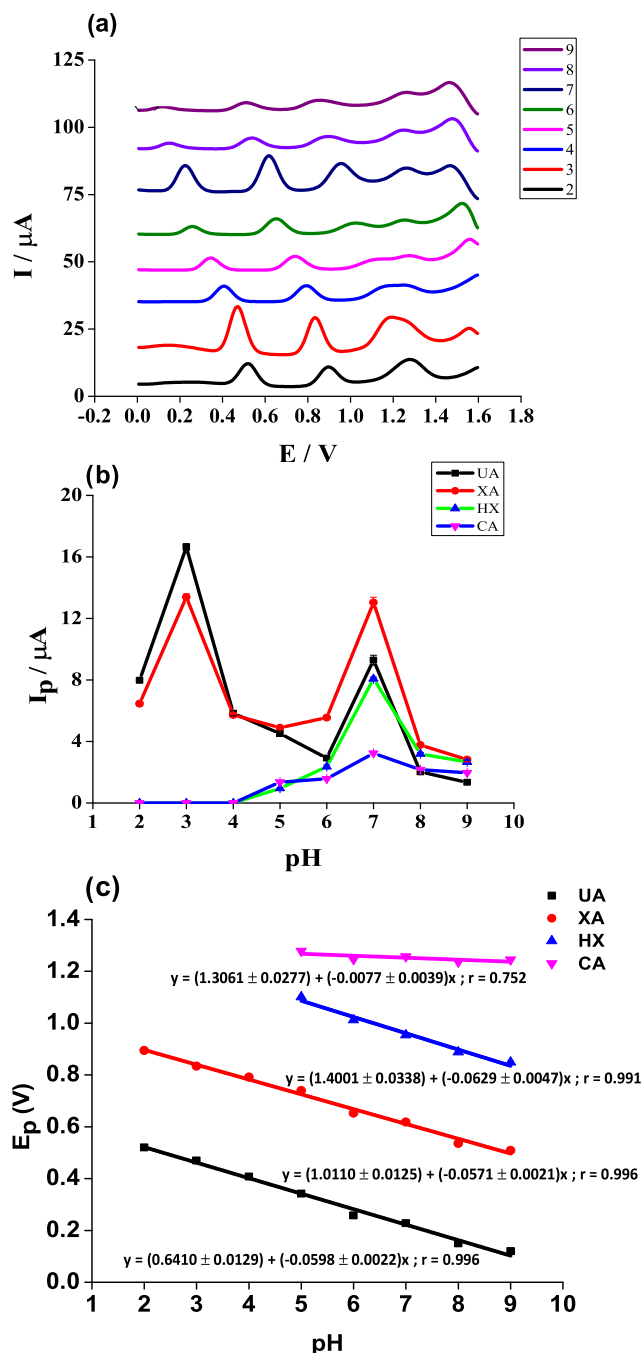


Figure 6. (a) DP-ASV voltammograms and (b) peak intensity (I_p) at different pH values on the activated polythiophene-wrapped chitosan/GCE. The accumulation experimental conditions are $t_{acc} = 10$ s, $E_{acc} = -0.9$ V, $\nu = 20$ mV s $^{-1}$. DP-ASV condition is $\Delta E = 60$ mV. (c) Linear regression equation representing the correlation between E_p (V) and pH of UA, XA, HX, and CA.

Although the electrochemical sensitivity of the polythiophene/chitosan nanocomposites is not significantly higher than those of some previously reported works,^{53–55} the modified electrodes described here can provide simultaneous analysis of four target analytes. The obtained sensing performance is good enough for implication in practice (that is, the excessively high sensitivity may cause unwanted interference and misdetection). We also found that the polythiophene/chitosan nanocomposite electrodes can be used repeatedly without regenerating or

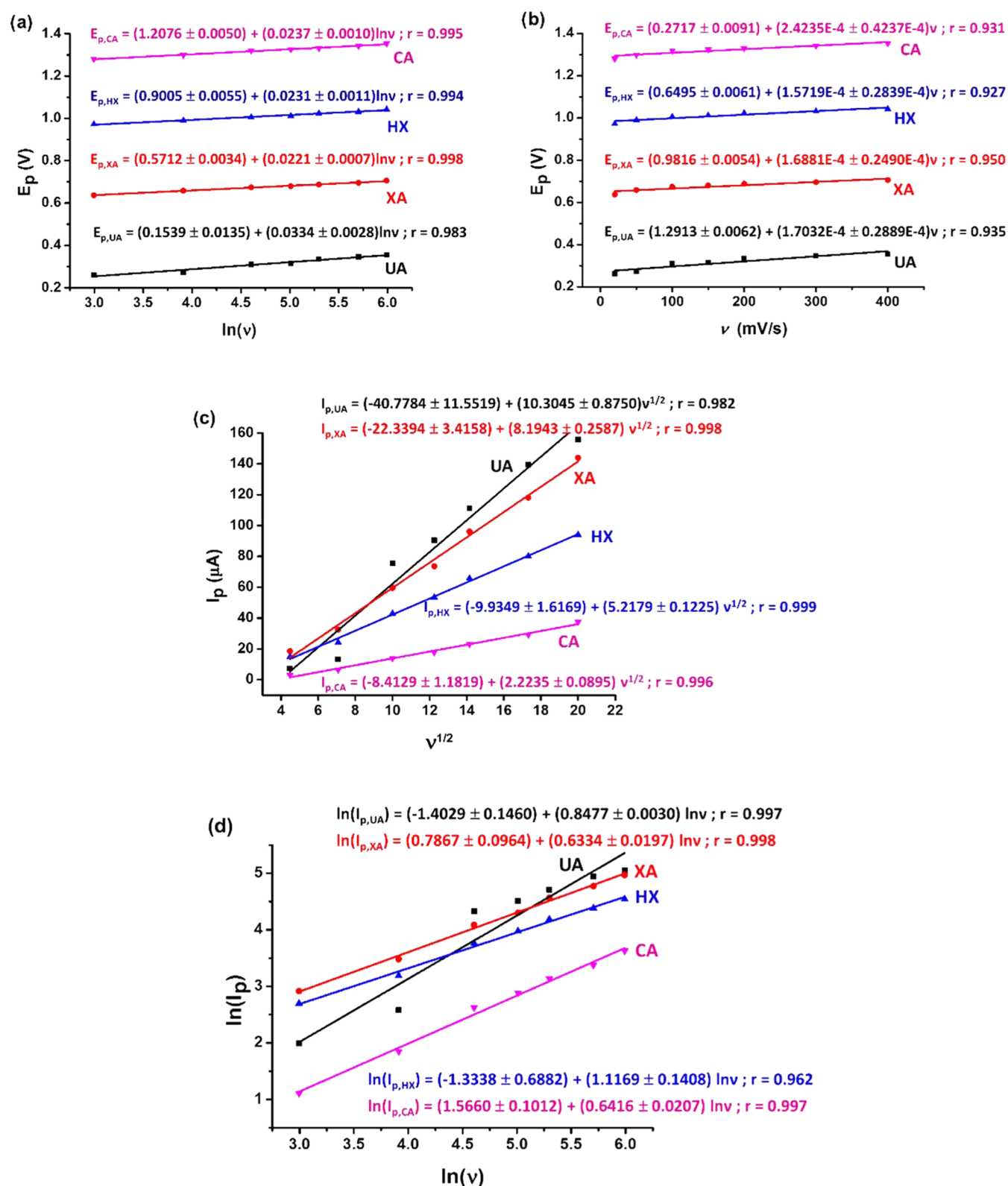


Figure 7. Linear regression equation representing the correlation between (a) E_p and $\ln(\nu)$, (b) E_p and ν , (c) I_p and $\nu^{1/2}$, and (d) $\ln(I_p)$ and $\ln(\nu)$ of UA, XA, HX, and CA.

reactivating the surface between successive determinations and can also be used for a long total experimental time.

We also investigated the influence of the different scan rates (ν) on the electrochemical response of UA, XA, HX, and CA at the polythiophene-wrapped chitosan/GCE electrode (Figure

7). The plots of the peak potential (E_p) as a function of ν for the four analytes are shown in Figure 7b. For all four compounds, the oxidation peak current linearly increases with increasing scan rate from 20 to 400 mV s^{-1} . This indicates that the electrochemical reaction of UA, XA, HX, and CA at the

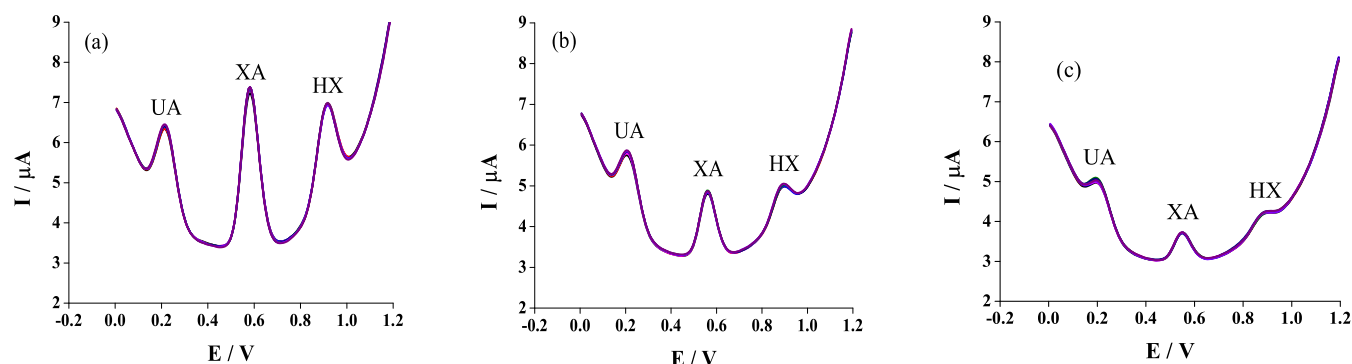


Figure 8. DP-ASV voltammograms of UA, XA, and HX at the three concentrations (a) 5 μM , (b) 10 μM , and (c) 50 μM .

activated polythiophene-wrapped chitosan/GCE electrode is a typical direct electrochemical process. In addition, it was observed that the oxidation peak potential (E_p) shifts to more positive potentials with the increasing scan rate for all of the species. The analysis of these data showed that the plot of E_p vs the logarithm of the scan rate is indicative of a linear relationship (Figure 7a). This suggests a kinetic limitation in the reaction between the oxidation sites and the modified electrode surface, and thus the electrocatalytic oxidation of UA, XA, HX, and CA is irreversible. The linear regression equation relating E_p to the scan rate over the range of 20–400 mV s^{-1} can be expressed in Figure 7b. These values reflect surface-controlled electrode processes.

Figure 7a shows the plot of E_p and the logarithm of the scan rate ($\ln \nu$). The electron-transfer coefficient (α_s) and electron-transfer rate constant (k_s) could be determined by Laviron theory. For the irreversible system, the slope of the linear regression equation between E_p and $\ln \nu$ is $RT/(1 - \alpha)nF$ expressed as the following equation:

$$E_p = E^0 - \frac{RT}{(1 - \alpha)nF} \ln \frac{RTk_s}{(1 - \alpha)nF} + \frac{RT}{(1 - \alpha)nF} \ln \nu$$

Where n is the electron-transfer number, R is the gas constant ($R = 8.314 \text{ J mol}^{-1} \text{ K}^{-1}$), T is the temperature in Kelvin ($T = 298 \text{ K}$), and F is the Faraday constant ($F = 96493 \text{ C mol}^{-1}$). α_s is calculated to be $\alpha_{\text{UA}} = 0.611$, $\alpha_{\text{XA}} = 0.416$, $\alpha_{\text{HX}} = 0.442$, and $\alpha_{\text{CA}} = 0.465$. These α_s values is similar to the results of Ojani et al.⁵⁶ (0.30 for UA, 0.36 for XA, and 0.62 for HX) and Wen et al.⁵⁷ (0.51 for UA, 0.46 for XA, and 0.36 for HX). The standard potential (E^0) of the associated redox pairs of UA, XA, HX, and CA compared with the silver reference electrode ($\text{Ag} | \text{AgCl} (r) | 1 \text{ M KCl}$) is the intercept of the linear regression equation between E_p and ν , which is +0.272, +0.650, +0.982, and +1.291 V, respectively. The k_s values of UA, HX, XA, and CA are calculated to be 1082, 1649, 1471, and 1324 s^{-1} , respectively. The k_s values according to UA, XA, HX, and CA in this work are higher than the results of others such as Yang et al.⁵⁸ (733 s^{-1}), Soleymani et al.⁵⁹ (202 s^{-1}), and Ojani et al.⁵⁶ (210 s^{-1}). This revealed that the speed of electron transfer on the modified electrode surface is fast enough to reflect the origin of the good conductivity and the permeable structure of the polythiophene/chitosan assembled nanocomposites.^{60,61}

The correlation between I_p vs $\nu^{1/2}$ and $\ln(I_p)$ vs $\ln(\nu)$ (Figure 7c,d) presents more information about the reversibility of the reactions and the behavior of the electrochemical process occurring at the surface of the anode electrode. Figure 7c shows the plots of I_p vs $\nu^{1/2}$ of the four analytes to be linear and do not cross the origin of the axes. This reveals that the electrooxidation

anodic processes proceeded by electrochemical reactions followed by homogeneous chemical reactions. This could also be observed by the slope of the plot of $\ln(I_p)$ vs $\ln(\nu)$ (Figure 7d), where the obtained slope values are 1.117 (± 0.141), 0.642 (± 0.019), 0.633 (± 0.020), and 0.848 (± 0.030) for UA, XA, HX, and CA, respectively. These slopes close to 0.5 are characteristic of the diffusion-controlled process, otherwise those close to 1 are ascribed to the adsorption-controlled process.^{62,63} These results indicate that the electron transfer process could be controlled by adsorption for UA, and by both the diffusion and adsorption control for XA, HX, and CA.

These results can be explained by forming hydrogen bonding between the hydroxyl and amine groups in the polythiophene/chitosan and the carbonyl, hydroxyl, and amide groups in UA, XA, HX, and CA. The adsorption process on the electrode is thus the chemical adsorption process formed by hydrogen bonding between the analytes and the material-coated electrode. The functional surface groups in the analytes and polythiophene/chitosan composite materials could contribute to the formation of hydrogen bonding. These chemical behaviors can anticipate that the adsorption process is more dominant for HX and gradually decreases from UA to XA and CA.

To be able to apply PTh-CTS(act)/GCE to analyze real samples, it is necessary to evaluate the reliability of the method including repeatability, linear range, limit of detection (LOD), and limit of qualification (LOQ). Due to the low signal of CA, the repeatability of the PTh-CTS(act)/GCE anodization process was investigated by an eight times repetitive voltammetric sweep for the 5, 10, and 50 μM solutions of HX, XA, and UA (Figure 8). The percentage of the relative standard deviation (RSD) values were calculated as 1.30, 0.94, and 2.01% for HX, XA, and UA, respectively, when the analyte concentrations were 5 μM . When a concentration of 10 μM of each analyte was used, calculated values were 1.64, 1.50, and 3.46% for HX, XA, and UA, respectively. And when the experiment was conducted on the 50 μM solutions of HX, XA, and UA, the calculated values were 4.25, 1.74, and 4.90%, respectively. On the other hand, comparing RSD in experiments with $1/2\text{RSD}_H$ at corresponding concentrations shows that all RSD values are smaller than the $1/2\text{RSD}_H$ value. The above results show that the PTh-CTS(act)/GCE modified electrode has good repeatability for the three substances UA, XA, and HX simultaneous voltammetric measurement, ranging from 0.94 to 4.89%.

Determination of the linear range of the DP-ASV method using the PTh-CTS(act)/GCE modified electrode for UA, XA, and HX was carried out by the simultaneous addition of all three

analytes UA and HX. The results are presented in Table 2 and Figure 9.

Table 2. I_p Values of UA, XA, and HX at Different Simultaneous Addition Concentrations

| C (μM) | UA | | XA | | HX | |
|-----------------------|-------------------------|---------|-------------------------|---------|-------------------------|---------|
| | I_p (μA) | RSD (%) | I_p (μA) | RSD (%) | I_p (μA) | RSD (%) |
| 2 | 0.3008 | 10.90 | 0.3348 | 2.98 | 0.0767 | 13.97 |
| 4 | 0.4818 | 6.55 | 0.5929 | 2.29 | 0.1976 | 9.46 |
| 6 | 0.6448 | 5.30 | 0.8147 | 1.73 | 0.3033 | 1.94 |
| 8 | 0.8113 | 4.65 | 0.9937 | 2.76 | 0.3726 | 2.81 |
| 10 | 0.9140 | 5.03 | 1.198 | 2.62 | 0.4812 | 7.28 |
| 25 | 1.451 | 2.17 | 2.303 | 1.45 | 1.217 | 2.76 |
| 50 | 1.877 | 1.49 | 3.582 | 0.85 | 2.101 | 1.17 |
| 75 | 2.177 | 1.67 | 4.490 | 0.92 | 2.826 | 0.88 |
| 100 | 2.303 | 3.56 | 5.081 | 1.15 | 3.240 | 2.87 |

The results reveal that there are two linear ranges for each analyte UA, XA, and HX with large correlation coefficients (0.955–0.998) corresponding to two concentration ranges of (1), (3), and (5) from 10 to 100 μM and (2), (4), and (6) from 2 to 10 μM . The corresponding linear equations are determined as follows:

$$\text{UA: } I_{p1,UA} = (0.164 \pm 0.027) + (77 \pm 788)C_{UA}; \quad r = 0.996 \quad (1)$$

$$I_{p2,UA} = (0.149 \pm 0.028) + (106 \pm 311)C_{UA}; \quad r = 0.998 \quad (2)$$

$$\text{XA: } I_{p1,XA} = (-0.009 \pm 0.016) + (49 \pm 202)C_{XA}; \quad r = 0.996 \quad (3)$$

$$I_{p2,XA} = (0.971 \pm 0.163) + (14 \pm 881)C_{XA}; \quad r = 0.955 \quad (4)$$

$$\text{HX: } I_{p1,HX} = (1.111 \pm 0.294) + (42 \pm 685)C_{HX}; \quad r = 0.981 \quad (5)$$

$$I_{p2,HX} = (0.380 \pm 0.186) + (30 \pm 625)C_{HX}; \quad r = 0.986 \quad (6)$$

Determination of the LOD and LOQ of the DP-ASV method using the PTh-CTS(act)/GCE electrode was started from the linear range results, by narrowing the concentration range of UA, XA, and HX in the case of adding individual standards of each analyte. Perform the experiments with the concentration of the analytes ranging from 2 to 10 μM . Using linear equations representing the correlation between I_p and the concentrations of three analytes (2), (4), and (6), the LOD and LOQ values were calculated to be 1.01 and 3.03–4.04 μM for UA, 1.06 and 3.18–4.24 μM for XA, 0.45 μM , and 1.35–1.80 μM for HX, respectively. These results indicated that the DP-ASV method using the PTh-CTS(act)/GCE modified electrode for the determination of UA, XA, and HX was able to analyze real samples due to a wide linear range and a low LOD.

CONCLUSIONS

In summary, our experiments provide inspiration for the host–guest complexation of thiophene and chitosan to fabricate biomimetic polythiophene-wrapped chitosan composite membranes with electrochemical properties. The discarded crab shells were used as a starting source to extract chitin that underwent alkali-induced deacetylation to convert it to a hierarchical chitosan structure. These extracted chitosan nanofibrils are iridescent macroscopic membranes with a Bouligand structure and mechanical flexibility, which are beneficial as a photonic platform for developing secondary materials. Taking the uniqueness of the hierarchically layered assemblies at the nanoscale, we homogeneously incorporated polythiophene into chitosan networks to obtain electrochemical composite membranes. We designed the polythiophene/chitosan-modified glassy carbon electrode and integrated it into a three-electrode system, which allowed us to analyze four organic compounds (uric acid, xanthine, hypoxanthine, and caffeine) at one time. Beyond the structural inhomogeneity of conventional chitosan, the inspirational research of the fascinating type of Bouligand structure exclusively endows the naturally assembled chitosan membranes with remarkable

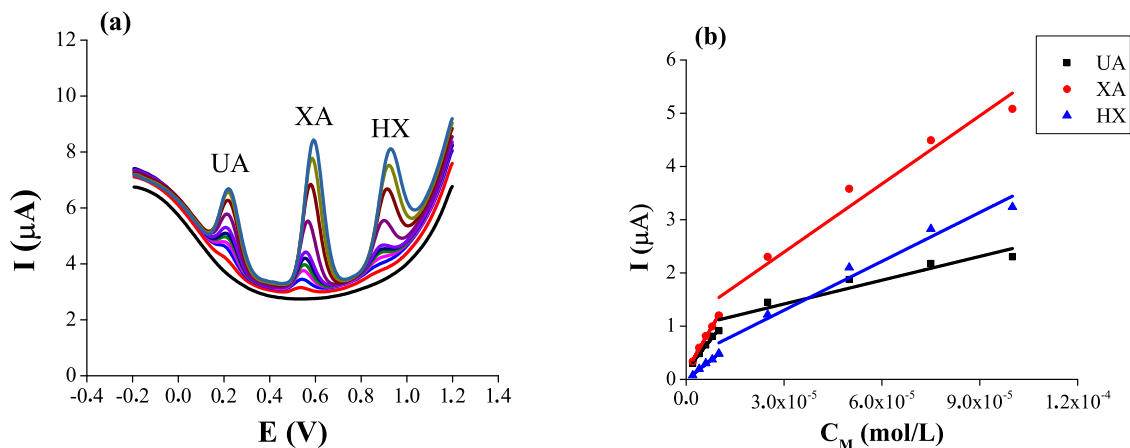


Figure 9. (a) DP-ASV voltammograms of UA, XA, and HX at different simultaneous addition concentrations and (b) linear equations between I_p and concentration of UA, XA, and HX.

mechanical, optical, and support functionalities in developing biomimetic materials to boost new applications. Since both thiophene and chitosan serving as conducting carbon precursors are active components for energy storage materials, our prepared polythiophene/chitosan composites could be used as promising carbonized precursors for further investigating energy applications in supercapacitors, lithium-ion batteries, and electrochemical catalysts.

METHODS

Chemicals. Discarded shells of the cooked crabs (*Scylla olivacea*) were collected from local seafood restaurants. Thiophene, ammonium persulfate, HX, XA, UA, and CA were purchased from Sigma Aldrich; and thiophene was distilled prior to use. Boric acid, acetic acid, phosphoric acid, disodium hydrophosphate, sodium dihydrophosphate, hydrochloric acid, sodium hydroxide, and ethanol were received from Xilong Scientific Co. Nafion aqueous dispersion (10 wt % in H₂O) was purchased from Sigma Aldrich

Preparation of Polythiophene-wrapped Chitosan Composite Membranes. *Preparation of Twisted Bouligand Chitosan Membranes.* Discarded crab shells were cleaned by washing with copious water and dried at room temperature for material preparation. The iridescent chitosan membranes were prepared according to our previous report.³¹ The cleaned crab shells (~12 g) were treated with NaOH_(aq) (250 mL, 5 wt %) at 90 °C for 6 h to decompose protein and then treated with HCl_(aq) (250 mL, 0.1 M) at ambient conditions for 24 h to dissolve calcium-based minerals. Purified chitin shells were obtained after washing with copious water. The resulting chitin (~3.5 g) was soaked in NaOH_(aq) (500 mL, 50 wt %) and heated at 90 °C for 8 h to proceed the deacetylation. This reaction was repeated three times to maximize the deacetylation of the chitin nanofibrils. The fully deacetylated product was washed thoroughly with deionized water to obtain free-standing iridescent chitosan membranes.

Preparation of Polythiophene-wrapped Chitosan Composite Membranes. 1.3 mL of thiophene was mixed with 20 mL of distilled water in a two-neck flask and sonicated for 30 min. The prepared helicoidal chitosan membranes (250 mg) were added to the above solution followed by drop-casting of 20 mL of 0.91 M ammonium persulfate. The reaction mixture was heated to 60 °C to facilitate the oxidative polymerization of thiophene into polythiophene onto chitosan nanofibrils. After 6 h, polythiophene-wrapped chitosan composites were isolated, immersed in ethanol, and then dried at 50 °C to obtain black membranes.

Structural Characterization. Powder X-ray diffraction (PXRD) patterns of the samples were recorded on an Advance Bruker D8 X-ray diffractometer. Scanning electron microscopy (SEM) images of the samples were obtained on a JSM-6490LV electron microscope. Samples were prepared by attaching them to aluminum stubs using double-sided adhesive tape and sputter coating with Pt–Pd (8 nm). Transmission electron microscopy images of the samples were obtained on a JEOL-JEM 1010 electron microscope. Energy-dispersive X-ray (EDX) analysis was collected using a Hitachi S2300 scanning electron microscope. Thermogravimetric analysis (TGA) of the samples (~10 mg) was conducted at a heating rate of 10 °C min⁻¹ under air atmosphere from RT to 800 °C using a Labsys TG/DSC-SETARAM thermogravimetric analyzer. Infrared spectra were obtained on neat samples using an IR-Prestige-21 spectrometer.

Electrochemical Experiments. *Apparatus.* Cyclic voltammetry (CV) and differential pulse anodic stripping voltammetry

(DP-ASV) measurements were performed using a CPA-HHS computerized polarography analyzer with a three-electrode system including a glassy carbon electrode, an Ag|AgCl (1 M KCl) electrode, and a platinum wire as a working electrode (WE), a reference electrode (RE), and a counter electrode (CE), respectively.

Preparation of Polythiophene-wrapped Chitosan-Modified GCE. Prior to use, a 2.8 mm-diameter GCE was fully polished with 0.05 μm alumina slurry on a cloth and rinsed with double distilled water to remove external contaminants. The cleaned GCE was immersed in a 2.0 M HNO₃ solution for 1 h, rinsed with distilled water followed by alcohol, and then dried at ambient conditions. For the preparation of polythiophene-wrapped chitosan-modified GCE, 0.20 g of polythiophene/chitosan was finely ground into powder and dispersed in 100 mL of 0.1 M acetic acid solution by sonication. Five μL of Nafion dispersion was then added to enhance the stability of the modified electrode. Subsequently, 2.5 μL of the dispersion was drop cast on the pretreated GCE surface, which was dried at ambient conditions to obtain polythiophene/chitosan-modified GCE (PTh-CTS/GCE). The polythiophene/chitosan-modified GCE was converted to activated polythiophene/chitosan-modified GCE (PTh-CTS(act)/GCE) by using the CV method in 0.04 M Britton–Robinson buffer (BRB, pH 7.0) with a scan rate of 50 mV s⁻¹, a sweep range of 0.0–1.7 V, and 9 cycles. After the electrochemical reaction was completed, PTh-CTS(act)/GCE was rinsed with distilled water.

Electrochemical Measurements. The experiments were carried out at room temperature using the DP-ASV method. The PTh-CTS(act)/GCE was immersed in 10 mL of 0.04 M BRB (pH 7.0) containing HX, XA, UA, and CA at certain concentrations. DP-ASV was recorded in a sweep range varying from 0.00 to 1.60 V at a scan rate (ν) of 200 mV s⁻¹ with an accumulation potential (E_{acc}) of -600 mV, accumulation time (t_{acc}) of 10 s, and a differential pulse amplitude (ΔE) of 0.07 V.

AUTHOR INFORMATION

Corresponding Author

Nhan Thi Thanh Dang – Department of Chemistry, Hue University of Education, Hue University, Hue 530000, Vietnam; orcid.org/0000-0002-9873-6731; Email: nhandang@hueuni.edu.vn

Authors

Thang Quoc Le – Department of Chemistry, Hue University of Education, Hue University, Hue 530000, Vietnam

Nguyen Duc Cuong – Department of Chemistry, Hue University of Education, Hue University, Hue 530000, Vietnam; orcid.org/0000-0002-7341-3661

Nguyen Le My Linh – Department of Chemistry, Hue University of Education, Hue University, Hue 530000, Vietnam

Lam Son Le – Department of Chemistry, Hue University of Sciences, Hue University, Hue 530000, Vietnam

Tien Dong Tran – Department of Chemistry, Hue University of Education, Hue University, Hue 530000, Vietnam

Hai Phong Nguyen – Department of Chemistry, Hue University of Sciences, Hue University, Hue 530000, Vietnam

Complete contact information is available at:

<https://pubs.acs.org/10.1021/acsomega.3c07894>

Notes

The authors declare no competing financial interest.

ACKNOWLEDGMENTS

This work was supported by the Hue University of Education, Hue University [Grant Number TN21-NCM-03]; N.T.T.D. is grateful to Dr. Thanh-Dinh Nguyen (University of British Columbia, Canada) for valuable discussions and motivation.

REFERENCES

- (1) Someya, T.; Bao, Z.; Malliaras, G. G. The rise of plastic bioelectronics. *Nature* **2016**, *540*, 379–385.
- (2) Fahlman, M.; Fabiano, S.; Gueskine, V.; Simon, D.; Berggren, M.; Crispin, X. Interfaces in organic electronics. *Nat. Rev. Mater.* **2019**, *4*, 627–650.
- (3) Namsheer, K.; Rout, C. S. Conducting polymers: a comprehensive review on recent advances in synthesis, properties and applications. *RSC Adv.* **2021**, *11*, 5659–5697.
- (4) Li, C.; Bai, H.; Shi, G. Conducting polymer nanomaterials: electrosynthesis and applications. *Chem. Soc. Rev.* **2009**, *38*, 2397–2409.
- (5) Wang, L.; Lin, J.; Zhang, X. Hierarchical microstructures self-assembled from polymer systems. *Polymer* **2013**, *54*, 3427–3442.
- (6) Sang, Y.; Liu, M. Hierarchical self-assembly into chiral nanostructures. *Chem. Sci.* **2022**, *13* (3), 633–656.
- (7) Allison, L.; Hoxie, S.; Andrew, T. L. Towards seamlessly-integrated textile electronics: Methods to coat fabrics and fibers with conducting polymers for electronic applications. *Chem. Commun.* **2017**, *53*, 7182–7193.
- (8) Alcaraz-Espinoza, J. J.; De Melo, C. P.; De Oliveira, H. P. Fabrication of Highly Flexible Hierarchical Polypyrrole/Carbon Nanotube on Eggshell Membranes for Supercapacitors. *ACS Omega* **2017**, *2* (6), 2866–2877.
- (9) Pasparakis, G.; Krasnogor, N.; Cronin, L.; Davis, B. G.; Alexander, C. Controlled polymer synthesis—from biomimicry towards synthetic biology. *Chem. Soc. Rev.* **2010**, *39*, 286–300.
- (10) Liu, Y.-F.; Huang, P.; Li, Y.; et al. A biomimetic multifunctional electronic hair sensor. *J. Mater. Chem. A* **2019**, *7*, 1889–1896.
- (11) Hazra, S.; Banerjee, A.; Nandi, A. K. Organic Mixed Ion-Electron Conductivity in Polymer Hybrid Systems. *ACS Omega* **2022**, *7* (37), 32849–32862.
- (12) McCullough, R. D. The Chemistry of Conducting Polythiophenes. *Adv. Mater.* **1998**, *10* (2), 93–116.
- (13) Kaloni, T. P.; Giesbrecht, P. K.; Schreckenbach, G.; Freund, M. S. Polythiophene: From Fundamental Perspectives to Applications. *Chem. Mater.* **2017**, *29*, 10248–10283.
- (14) Guo, X.; Baumgarten, M.; Müllen, K. Designing π -conjugated polymers for organic electronics. *Prog. Polym. Sci.* **2013**, *38* (12), 1832–1908.
- (15) Thanasamy, D.; Jesuraj, D.; Konda Kannan, S. K.; Avadhanam, V. A novel route to synthesis polythiophene with great yield and high electrical conductivity without post doping process. *Polymer* **2019**, *175*, 32–40.
- (16) Cabuk, M.; Yavuz, M.; Unal, H. I.; Alan, Y. Synthesis, Characterization, and Enhanced Antibacterial Activity of Chitosan-Based Biodegradable Conducting Graft Copolymers. *Polym. Compos.* **2014**, *2014* (2), 497–509.
- (17) Lan, D.; Zhang, L. Electrochemical synthesis of a novel purine-based polymer and its use for the simultaneous determination of dopamine, uric acid, xanthine and hypoxanthine. *J. Electroanal. Chem.* **2015**, *757*, 107–115.
- (18) Pérez-Madrigal, M. M.; Armelin, E.; Puiggali, J.; Alemán, C. Insulating and semiconducting polymeric free-standing nanomembranes with biomedical applications. *J. Mater. Chem. B* **2015**, *3* (29), 5904–5932.
- (19) Wijeratne, K.; Ail, U.; Brooke, R.; et al. Bulk electronic transport impacts on electron transfer at conducting polymer electrode–electrolyte interfaces. *Proc. Natl. Acad. Sci. U.S.A.* **2018**, *115* (47), 11899–11904.
- (20) Inoue, A.; Yuk, H.; Lu, B.; Zhao, X. Strong adhesion of wet conducting polymers on diverse substrates. *Sci. Adv.* **2020**, *6* (12), No. eaay5394, DOI: 10.1126/sciadv.aay5394.
- (21) Ak, M.; Ak, M. S.; Toppare, L. Electrochemical properties of a new star-shaped pyrrole monomer and its electrochromic applications. *Macromol. Chem. Phys.* **2006**, *207* (15), 1351–1358.
- (22) Khan, A.; Jain, R. K.; Banerjee, P.; et al. A hybrid electro-responsive SWNT/PEDOT: PSS-based membrane towards soft actuator applications. *J. Reinf. Plast. Compos.* **2021**, *40* (3–4), 87–102.
- (23) Nair, S. S.; Mishra, S. K.; Kumar, D. Recent progress in conductive polymeric materials for biomedical applications. *Polym. Adv. Technol.* **2019**, *30* (12), 2932–2953.
- (24) Khan, F.; Tanaka, M.; Ahmad, S. R. Fabrication of polymeric biomaterials: a strategy for tissue engineering and medical devices. *J. Mater. Chem. B* **2015**, *3* (42), 8224–8249.
- (25) Zhao, Z.; Richardson, G. F.; Meng, Q.; Zhu, S.; Kuan, H. C.; Ma, J. PEDOT-based composites as electrode materials for supercapacitors. *Nanotechnology* **2016**, *27* (4), No. 042001, DOI: 10.1088/0957-4484/27/4/042001.
- (26) Han, G.; Shi, G. Conducting polymer electrochemical actuator made of high-strength three-layered composite films of polythiophene and polypyrrole. *Sens. Actuators, B* **2004**, *99*, 525–531.
- (27) Miller, A. J.; Hatton, R. A.; Silva, S. R. P. Water-soluble multiwall-carbon- nanotube-polythiophene composite for bilayer photovoltaics. *Appl. Phys. Lett.* **2006**, *89* (12), No. 123115.
- (28) Qiu, L.; Lee, W. H.; Wang, X.; et al. Organic Thin-film Transistors Based on Polythiophene Nanowires Embedded in Insulating Polymer. *Adv. Mater.* **2009**, *21*, 1349–1353.
- (29) Zhang, X.; Rolandi, M. Engineering strategies for chitin nanofibers. *J. Mater. Chem. B* **2017**, *5* (14), 2547–2559.
- (30) Nguyen, T. D.; Peres, B. U.; Carvalho, R. M.; MacLachlan, M. J. Photonic Hydrogels from Chiral Nematic Mesoporous Chitosan Nanofibril Assemblies. *Adv. Funct. Mater.* **2016**, *26*, 2875–2881.
- (31) Dang, N. T. T.; Chau, T. T. L.; Duong, H. Van.; et al. Water-soluble chitosan-derived sustainable materials: Towards filaments, aerogels, microspheres, and plastics. *Soft Matter* **2017**, *13* (40), 7292–7299.
- (32) Van Duong, H.; Chau, T. T. L.; Dang, N. T. T.; et al. Biocompatible Chitosan-Functionalized Upconverting Nanocomposites. *ACS Omega* **2018**, *3* (1), 86–95.
- (33) Kumar, R.; Ranwa, S.; Kumar, G. Biodegradable Flexible Substrate Based on Chitosan/PVP Blend Polymer for Disposable Electronics Device Applications. *J. Phys. Chem. B* **2020**, *124* (1), 149–155.
- (34) Saravanan, S.; Leena, R. S.; Selvamurugan, N. Chitosan based biocomposite scaffolds for bone tissue engineering. *Int. J. Biol. Macromol.* **2016**, *93*, 1354–1365.
- (35) Rabea, E. I.; Badawy, M. E. T.; Stevens, C. V.; Smagge, G.; Steurbaut, W. Chitosan as Antimicrobial Agent: Applications and Mode of Action. *Biomacromolecules* **2003**, *4* (6), 1457–1465.
- (36) Cabuk, M.; Yavuz, M.; Unal, H. I. Electrokinetic, electro-rheological and viscoelastic properties of Polythiophene-graft-Chitosan copolymer particles. *Colloids Surf., A* **2016**, *510*, 231–238.
- (37) Bagheri, H.; Roostaie, A.; Baktash, M. Y. A chitosan-polypyrrole magnetic nanocomposite as μ -sorbent for isolation of naproxen. *Anal. Chim. Acta* **2014**, *816*, 1–7.
- (38) Karthik, R.; Meenakshi, S. Removal of Pb(II) and Cd(II) Ions from Aqueous Solution Using Polyaniline Grafted Chitosan. *Chem. Eng. J.* **2015**, *263*, 168–177, DOI: 10.1016/j.cej.2014.11.015.
- (39) Nezakati, T.; Seifalian, A.; Tan, A.; Seifalian, A. M. Conductive Polymers: Opportunities and Challenges in Biomedical Applications. *Chem. Rev.* **2018**, *118* (14), 6766–6843.
- (40) Ramdzan, N. S. M.; Fen, Y. W.; Anas, N. A. A.; Omar, N. A. S.; Saleviter, S. Development of biopolymer and conducting polymer-based optical sensors for heavy metal ion detection. *Molecules* **2020**, *25* (11), 2548–2573.
- (41) Idumah, C. I. Novel trends in conductive polymeric nanocomposites, and bionanocomposites. *Synth. Met.* **2021**, *273*, No. 116674.

- (42) Nawrot, P.; Jordan, S.; Eastwood, J.; Rotstein, J.; Hugenholz, A.; Feeley, M. Effects of caffeine on human health. *Food Addit. Contam.* **2003**, *20* (1), 1–30.
- (43) Raj, M. A.; John, S. A. Simultaneous determination of uric acid, xanthine, hypoxanthine and caffeine in human blood serum and urine samples using electrochemically reduced graphene oxide modified electrode. *Anal. Chim. Acta* **2013**, *771*, 14–20.
- (44) Sharma, V.; Crne, M.; Park, J. O.; Srinivasarao, M. Structural Origin of Circularly Polarized Iridescence in Jeweled Beetles. *Science* **2009**, *325*, 449–451.
- (45) Li, H.; Hu, C.; Yu, H.; Chen, C. Chitosan composite scaffolds for articular cartilage defect repair: A review. *RSC Adv.* **2018**, *8* (7), 3736–3749.
- (46) Chen, P. Y.; Lin, A. Y. M.; McKittrick, J.; Meyers, M. A. Structure and mechanical properties of crab exoskeletons. *Acta Biomater.* **2008**, *4* (3), 587–596.
- (47) Grunenfelder, L. K.; Herrera, S.; Kisailus, D. Crustacean-Derived Biomimetic Components and Nanostructured Composites. *Small* **2014**, *10* (16), 3207–3232.
- (48) Sumboja, A.; Liu, J.; Zheng, W. G.; Zong, Y.; Zhang, H.; Liu, Z. Electrochemical energy storage devices for wearable technology: a rationale for materials selection and cell design. *Chem. Soc. Rev.* **2018**, *47* (15), 5919–5945.
- (49) Lv, Z.; Li, W.; Yang, L.; Loh, X. J.; Chen, X. Custom-Made Electrochemical Energy Storage Devices. *ACS Energy Lett.* **2019**, *4* (2), 606–614.
- (50) Wolski, K.; Gruszkiewicz, A.; Zapotoczny, S. Conductive polythiophene-based brushes grafted from an ITO surface via a self-templating approach. *Polym. Chem.* **2015**, *6* (43), 7505–7513.
- (51) Eren, E.; Aslan, E.; Oksuz, A. U. The Effect of Anionic Surfactant on the Properties of Polythiophene/Chitosan Composites. *Polym. Eng. Sci.* **2014**, *54* (11), 2632–2640.
- (52) Bouligand, Y. Twisted fibrous arrangements in biological materials and cholesteric mesophases. *Tissue Cell* **1972**, *4* (2), 189–217.
- (53) Wang, Y.; Tong, L. Electrochemical sensor for simultaneous determination of uric acid, xanthine and hypoxanthine based on poly (bromocresol purple) modified glassy carbon electrode. *Sens. Actuators, B* **2010**, *150*, 43–49.
- (54) Pierini, G. D.; Robledo, S. N.; Zon, M. A.; Nezio, M. S. Di.; Granero, A. M.; Fernández, H. Development of an electroanalytical method to control quality in fish samples based on an edge plane pyrolytic graphite electrode. Simultaneous determination of hypoxanthine, xanthine and uric acid. *Microchem. J.* **2018**, *138*, 58–64.
- (55) Wang, Y. Simultaneous determination of uric acid, xanthine and hypoxanthine at poly (pyrocatechol violet)/functionalized multi-walled carbon nanotubes composite film modified electrode. *Colloids Surf., B* **2011**, *88*, 614–621.
- (56) Ojani, R.; Alinezhad, A.; Abedi, Z. A highly sensitive electrochemical sensor for simultaneous detection of uric acid, xanthine and hypoxanthine based on poly(L-methionine) modified glassy carbon electrode. *Sens. Actuators, B* **2013**, *188*, 621–630.
- (57) Wen, Y.; Chang, J.; Xu, L.; et al. Simultaneous voltammetric analysis of uric acid, xanthine and hypoxanthine using nanocomposite sensor based on carboxymethyl cellulose decorated both palygorskite and nitrogen doped graphene. *J. Electroanal. Chem.* **2017**, *805*, 159–170.
- (58) Yang, S.; Qu, L.; Yang, R.; Li, J.; Yu, L. Modified glassy carbon electrode with Nafion/MWNTs as a sensitive voltammetric sensor for the determination of paeonol in pharmaceutical and biological samples. *J. Appl. Electrochem.* **2010**, *40* (7), 1371–1378.
- (59) Soleymani, J.; Hasanzadeh, M.; Shadjou, N.; et al. A new kinetic-mechanistic approach to elucidate electrooxidation of doxorubicin hydrochloride in unprocessed human fluids using magnetic graphene based nanocomposite modified glassy carbon electrode. *Mater. Sci. Eng. C* **2016**, *61*, 638–650.
- (60) Chen, Z.; Vannucci, A. K.; Concepcion, J. J.; Jurss, J. W.; Meyer, T. J. Proton-coupled electron transfer at modified electrodes by multiple pathways. *Proc. Natl. Acad. Sci. U.S.A.* **2011**, *108* (52), 1461–1469.
- (61) Royea, W. J.; Hamann, T. W.; Brunshwig, B. S.; Lewis, N. S. A comparison between interfacial electron-transfer rate constants at metallic and graphite electrodes. *J. Phys. Chem. B* **2006**, *110* (39), 19433–19442.
- (62) Elgrishi, N.; Rountree, K. J.; McCarthy, B. D.; Rountree, E. S.; Eisenhart, T. T.; Dempsey, J. L. A Practical Beginner's Guide to Cyclic Voltammetry. *J. Chem. Educ.* **2018**, *95* (2), 197–206.
- (63) Garrido, J. A.; Rodríguez, R. M.; Bastida, R. M.; Brillas, E. Study by cyclic voltammetry of a reversible surface charge transfer reaction when the reactant diffuses to the electrode. *J. Electroanal. Chem.* **1992**, *324* (1–2), 19–32.